



Molecular modelling of quinoline derivatives as telomerase inhibitors through 3D-QSAR, molecular dynamics simulation, and molecular docking techniques

Keerti Vishwakarma¹ · Hardik Bhatt¹

Received: 5 February 2020 / Accepted: 15 December 2020 / Published online: 7 January 2021

© The Author(s), under exclusive licence to Springer-Verlag GmbH, DE part of Springer Nature 2021

Abstract

Rising mortality due to cancer has led to the development and identification of newer targets and molecules to cure the disease. Telomerase is one of the attractive targets for design of many chemotherapeutic drugs. This research highlights the designing of novel telomerase inhibitors using ligand-based (3D-QSAR) and structure-based (molecular docking and molecular dynamics simulation) approaches. For the development of the 3D-QSAR model, 37 synthetic molecules reported earlier as telomerase inhibitors were selected from diversified literature. Three different alignment methods were explored; among them, distill alignment was found to be the best method with good statistical results and was used for the generation of QSAR model. Statistically significant CoMSIA model with a correlation coefficient (r^2_{ncv}) value of 0.974, leave one out (q^2) value of 0.662 and predicted correlation coefficient (r^2_{pred}) value of 0.560 was used for the analysis of QSAR. For the MDS study, A-chain of telomerase was stabilised for 50 ns with respect to 1-atm pressure, with an average temperature of 299.98 k and with potential energy of 1,145,336 kJ/m converged in 997 steps. Furthermore, the behaviour study of variants towards the target revealed that active variable gave better affinity without affecting amino acid sequences and dimensions of protein which was accomplished through RMSD, RMSF and Rg analysis. Results of molecular docking study supported the outcomes of QSAR contour maps as ligand showed similar interactions with surrounded amino acids which were identified in contour map analysis. The results of the comprehensive study might be proved valuable for the development of potent telomerase inhibitors.

Keywords Telomerase · CoMFA · CoMSIA · MDS · Molecular docking

Introduction

Telomerase is a ribonucleoprotein reverse transcriptase, consisting of telomerase reverse transcriptional template RNA (hTR), telomerase reverse transcriptase (hTERT) and related protein [1, 2]. It has already been identified that 85–90% of cancer cells show overexpression of telomerase, which prevents telomere shorting and enables them to divide uncontrollably [3, 4]. Therefore, telomerase is an attractive oncological target that shows a distinctive role in cancer cell growth, high selectivity towards inhibitory mechanisms of cancer cell proliferation and multi-target ability.

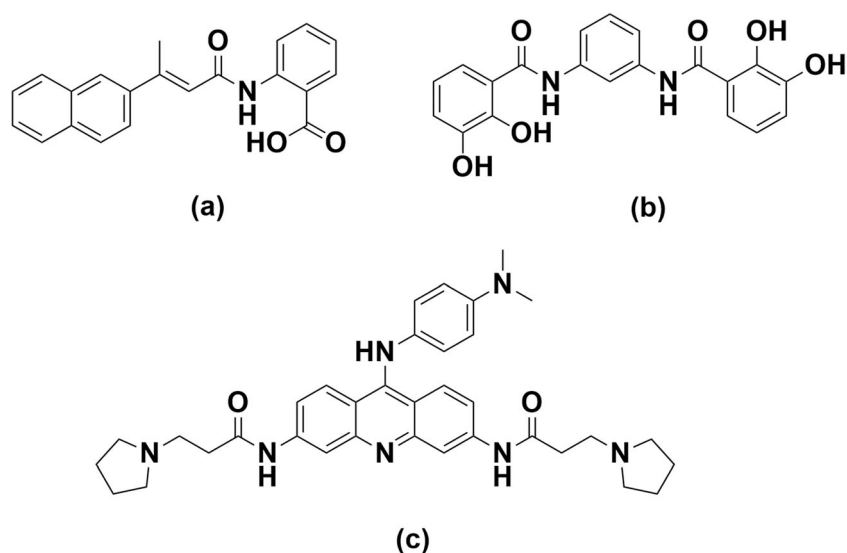
Multiple anti-telomerase approaches are explored in the form of chemotherapy, gene-therapy, immunotherapy, combination and stem cell therapy [5]. Additionally, G-quadruplex ligand-based and heat shock protein (HSP-90) inhibitors are reported as the mechanistic approach for targeting telomere [6]. Following the abovementioned approaches, various natural and synthetic heterocyclic moieties are identified as an anti-telomerase agents. Among all anti-telomerase agents, only few small molecules like BIBR1532 [7], MST-312 [8] and BARCO-19 [9] have reached in the pre-clinical trial stages, as shown in Fig 1. However, none of the above telomerase inhibitors is successful in getting the FDA approval until date; it might be due to lower potency, lower selectivity or toxicity constraints [10].

In this study, we performed structure-based and ligand-based drug design approaches for the identification of structural features of small molecules required for telomerase inhibition.

✉ Hardik Bhatt
hardikbhatt23@hotmail.com

¹ Department of Pharmaceutical Chemistry, Institute of Pharmacy, Nirma University, Ahmedabad 382481, India

Fig. 1 Telomerase inhibitors reported in the pre-clinical trial state



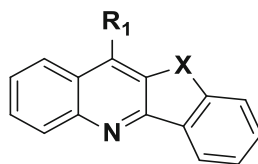
3D-QSAR is a ligand-based drug design approach used to generate a reliable statistical model for the prediction of the potency of new chemical entities [11]. It provided the correlation of molecular properties of the compound with its ligand-binding affinities [12]. CoMFA (Comparative Molecular Field Analysis) and CoMSIA (Comparative Molecular Similarity Indices Analysis) [13] are the most common and standard methods used for the development of the 3D-QSAR model [14]. In the CoMFA, columbic potential in terms of electrostatic field and Lennard-Jones potential in terms of the steric field are calculated. Like the CoMFA, the CoMSIA also helps to evaluate both the electrostatic and steric fields of the molecule, and additionally, it involves hydrophobic, hydrogen bond donor (HBD) and hydrogen bond acceptor (HBA) fields [15]. The CoMSIA differentiated from CoMFA through the Gaussian function and the steepness of the Gaussian function is controlled by an attenuation factor α at 0.3 as a standard value [16].

MDS (molecular dynamics simulations)-aided molecular docking helps to validate the QSAR model [17]. The MDS studies are performed for the identification of stable conformation of protein that helps to understand the behaviour and activity of biomolecule [18]. During the simulation process, changes in protein conformation in the presence of potential energy, pressure and temperature are calculated with respect to time. The results of MDS studies are validated by RMSD (root-mean-square deviation) value, RMSF (root-mean-square fluctuations), Rg (radius of gyration) analysis and Ramachandran plot [19, 20]. RMSD is the similarity measure used for the tracking of protein modifications during molecular dynamic studies. RMSD helps in the comparative studies of structural change of simulated and unsimulated protein molecules, while the RMSF analysis is useful to calculate the flexibility of enzyme residues of the given target throughout the simulation. The findings of the RMSF analysis suggest

changes in protein flexibility pattern in the presence of analysed variants. Structural displacement of protein atoms from their common mass centre is measured by the Rg analysis and, therefore, the Rg analysis helps to describe the effect of MDS over the proteins dimension [21, 22]. Furthermore, the Ramachandran plot helps to analyse the change in the torsional angle between the amino acids of the protein due to molecular simulation. In addition to the results of MDS, molecular docking is performed to explore the possible interaction of inhibitors with the target protein [23, 24].

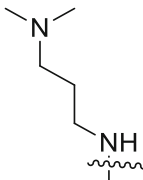
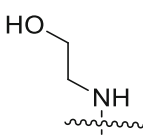
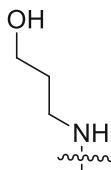
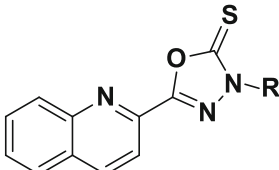
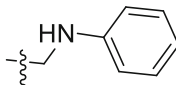
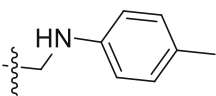
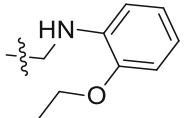
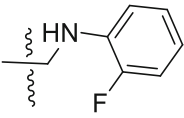
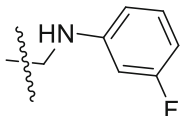
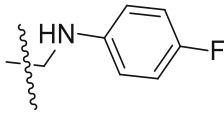
Materials and methods

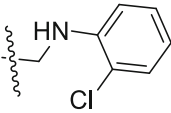
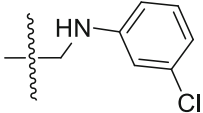
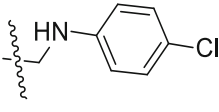
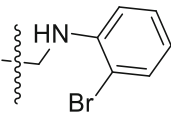
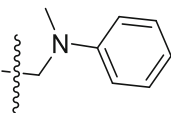
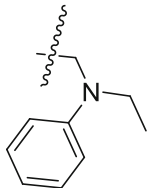
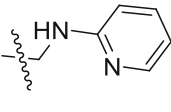
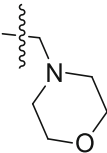
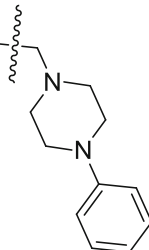
A data set of 37 synthetic molecules, reported as telomerase inhibitors in various literature, were selected for the development of the 3D-QSAR model, as shown in Table 1 [25–27]. Structures of all molecules were drawn and minimised by utilising tripose force field in SYBYL-X, and minimised charges were calculated through the Gasteiger-Huckel method. The reported IC_{50} values of all molecules were converted into pIC_{50} ($= -\log IC_{50}$) because pIC_{50} values traversed a wide range that help in the preparation of modified derivatives with enhanced activity [28]. This pIC_{50} was utilised as the dependent variable. Data set was divided into training set for the generation of the QSAR model and test set for validation of the QSAR model. In this work, 28 molecules were used as a training set and nine molecules were used as test set [75:25]. The selection of test and training set was carried out in such a manner that compounds of test set resembled the compounds of the training set in multi-dimensional descriptor space. Thus, a test set was a true demonstrator of a training set (mol 2 structures of all compounds are provided as [Supplementary Information data](#)).

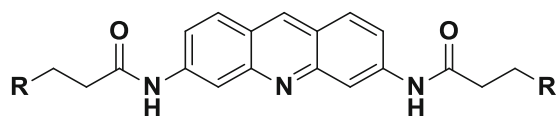
Table 1 Structure of telomerase inhibitors with biological activity

Compound No.	X	R	IC ₅₀ in μ M	pIC ₅₀
1*	N		0.55	6.2596
2	N		1.12	5.9508
3	N		0.44	6.3565
4	N		2.35	5.6289
5	N		1.55	5.8097
6*	O		4.38	5.3585
7	O		7.11	5.1481

*Test set molecules

8	O		3.29	5.4828
9	O		12.3	4.9101
10	O		8.12	5.0904
				
11*			12.8	4.8928
12			7.3	5.1367
13*			2.8	5.5528
14*			0.8	6.0969
15			1.1	5.9586
16			3.1	5.5086

17		5.5	5.2596
18*		3.0	5.5229
19		0.9	6.0458
20		10.8	4.9666
21*		9.3	5.0315
22		5.1	5.2924
23		3.1	5.5086
24*		2.9	5.5376
25		4.8	5.3188



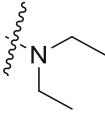
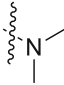
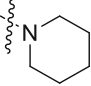
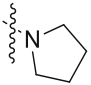
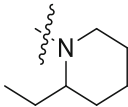
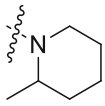
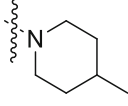
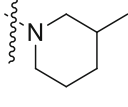
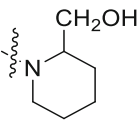
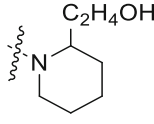
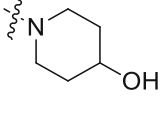
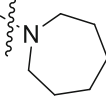
26		5.8	5.2366
27		8.2	5.0862
28		2.8	5.5528
29		5.2	5.2840
30		2.7	5.5686
31		2.6	5.5850
32*		1.35	5.8697
33		4.4	5.3565
34		5.4	5.2676
35		4.1	5.3872
36		8	5.0969
37		3.1	5.5086

Table 2 Statistical results of CoMFA and CoMSIA models by PLS analysis using three different alignment methods

Statistical parameter	Alignment I (distill alignment)		Alignment II (docking alignment)		Alignment III (pharmacophore alignment)	
	CoMFA	CoMSIA	CoMFA	CoMSIA	CoMFA	CoMSIA
NC	6	6	6	6	6	6
r^2_{ncv}	0.983	0.974	0.977	0.928	0.988	0.996
q^2	0.476	0.662	- 0.466	- 0.629	0.071	0.285
SEE	0.051	0.063	0.060	0.105	0.043	0.026
r^2_{cv}	0.446	0.660	- 0.411	- 0.586	0.111	0.314
r^2_{bs}	0.986	0.981	0.991	0.970	0.992	0.996
r^2_{pred}	0.453	0.560	- 0.038	- 0.098	0.044	0.112
Contributors						
Steric	0.446	0.093	0.388	0.131	0.502	0.124
Electrostatic	0.554	0.217	0.612	0.203	0.498	0.213
Hydrophobic	-	0.193	-	0.213	-	0.206
HBD	-	0.384	-	0.261	-	0.348
HBA	-	0.113	-	0.192	-	0.109

NC number of components, r^2_{ncv} non-cross-validated correlation coefficient, q^2 cross-validated correlation coefficient, SEE standard error of estimation, r^2_{cv} cross-validation correlation coefficient, r^2_{bs} mean r^2 of bootstrap analysis (10 runs), HBD hydrogen bond donor, HBA hydrogen bond acceptor

Before starting the QSAR analysis, molecular alignments were performed, as revealed in Fig. 2. Molecular alignment is the key factor for generating a reliable model as it helps to generate a better statistical result [29, 30]. In the present study, distill- or rigid body-based, pharmacophore-based and docking-based alignments were performed to find out the best alignment method for the generation of the 3D-QSAR model. In distill alignment method (Fig. 2a), a common core moiety from the data set of all 37 molecules was identified. After the identification of common core, the highest active molecule from the data set, viz. molecule 3, was selected as a template molecule and the rest molecules of data set were aligned over this template. In pharmacophore-based alignment (Fig. 2b), different conformers of every molecule were generated with the help of DISCOtech module of SYBYL-X. Conformers were aligned over each other for the generation of a common pharmacophore. Docking-based alignment (Fig. 2c) was carried out with the help of the Surflex module of SYBYL-X, in which ligand of telomerase (PDB ID 5CQG) [31] was selected from RCSB-PDB. A binding pocket was generated into the

ligand structure by protomol generation technique, and all molecules were docked in the binding pocket. From all these alignment techniques, distill alignment gave better statistical results as reported in Table 2, which was utilised for the development of a reliable 3D-QSAR model for further studies.

The CoMFA and CoMSIA were reported as efficient tools in ligand-based drug design which were used for contour map generation as well as for the identification of favourable and unfavourable regions in a moiety [32]. The CoMFA and CoMSIA of five defined fields were calculated at regular grid space of 2.0 Å in Cartesian directions and the grid points were generated using +1 charge as well as Vander Waal's radius of 1.52 Å. Energy cutoff for all fields was set as default at 30 kcal/mol. In the case of the CoMSIA study, the Gaussian function utilised for the determination of the distance between molecular atom and probe atom inside and outside of grid points [33].

For the estimation of linear correlation between structural parameters and biological activity, PLS (partial least squares) analysis was performed [34]. In the PLS analysis,

**Fig. 2** Different molecular alignments. **a** Distill alignment. **b** Pharmacophore alignment. **c** Docking alignment

Table 3 The predicted and experimental activity of the training and test set compounds for CoMFA and CoMSIA

Compound no.	Actual pIC ₅₀	Predicted pIC ₅₀ for CoMFA	Residual	Predicted pIC ₅₀ for CoMSIA	Residual
1*	6.2596	6.255	0.0046	6.074	0.1856
2	5.9508	5.57	0.3808	5.702	0.2488
3	6.3565	6.378	-0.0215	6.381	-0.0245
4	5.6289	5.637	-0.0081	5.614	0.0149
5	5.8097	5.795	0.0147	5.761	0.0487
6*	5.3585	5.455	-0.0965	5.369	-0.0105
7	5.1481	5.164	-0.0159	5.154	-0.0059
8	5.4828	5.453	0.0298	5.437	0.0458
9	4.9101	4.892	0.0181	4.9	0.0101
10	5.0904	5.162	-0.0716	5.18	-0.0896
11*	4.8928	5.504	-0.6112	5.516	-0.6232
12	5.1367	5.495	-0.3583	5.455	-0.3183
13*	5.5528	5.337	0.2158	5.282	0.2708
14*	6.0969	5.255	0.8419	5.256	0.8409
15	5.9586	5.96	-0.0014	5.939	0.0196
16	5.5086	5.555	-0.0464	5.553	-0.0444
17	5.2596	5.223	0.0366	5.231	0.0286
18*	5.5229	5.463	0.0599	5.519	0.0039
19	6.0458	6.022	0.0238	6.071	-0.0252
20	4.9666	5.148	-0.1814	5.168	-0.2014
21*	5.0315	5.053	-0.0215	5.05	-0.0185
22	5.2924	5.287	0.0054	5.284	0.0084
23	5.5086	5.508	0.0006	5.486	0.0226
24*	5.5376	5.287	0.2506	5.336	0.2016
25	5.3188	5.329	-0.0102	5.318	0.0008
26	5.2366	5.245	-0.0084	5.231	0.0056
27	5.0862	5.075	0.0112	5.098	-0.0118
28	5.5528	5.569	-0.0162	5.541	0.0118
29	5.284	5.306	-0.022	5.269	0.015
30	5.5686	5.563	0.0056	5.563	0.0056
31	5.585	5.57	0.015	5.591	-0.006
32*	5.8697	5.621	0.2487	5.562	0.3077
33	5.3565	5.347	0.0095	5.374	-0.0175
34	5.2676	5.276	-0.0084	5.252	0.0156
35	5.3872	5.396	-0.0088	5.415	-0.0278
36	5.0969	5.069	0.0279	5.082	0.0149
37	5.5086	5.622	-0.1134	5.417	0.0916

*Test set molecules

pIC₅₀ values were used as dependent variables and the CoMFA/CoMSIA descriptors were employed as independent variables for the development of the 3D-QSAR model [35]. No validation (r^2), standard error of estimation (SEE), Fischer's statistic value (f), leave one out (q^2), cross-validation (r^2_{cv}) and boost strapping (r^2_{bs}) were calculated in the PLS analysis with an optimal number of components (N). After numerous trials, the best model was selected based on the highest q^2 value and the results

of the PLS analysis was validated through the estimation of predictive power (r^2_{pred}) of the best-generated model. The determination of r^2_{pred} was based on test set molecules by the following equation:

$$r^2_{pred} = 1 - (\text{PRESS}/\text{SD})$$

where PRESS is the sum of squared deviation between the actual and predicted biological activity (pIC₅₀) of the test set molecules [$\text{PRESS} = \sum(Y_{\text{predicted}} - Y_{\text{mean}})^2$] and the SD denotes the sum of squared deviation of the actual and

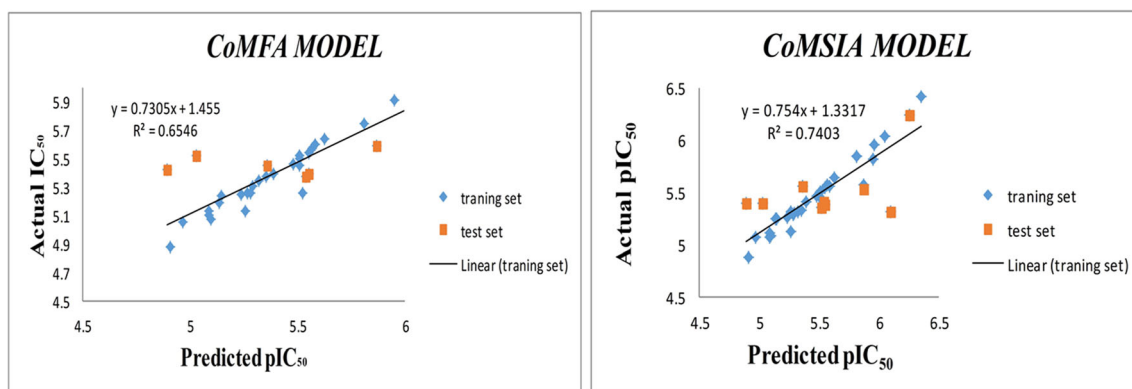


Fig. 3 Plot of experimental pIC_{50} versus predictive pIC_{50} of CoMFA and CoMSIA models.

predicted biological activity of training set molecules [$SD = \sum (Y_{actual} - Y_{mean})^2$]. The generated 3D-QSAR model having high predictive ability was confirmed based on high q^2 and r^2 values ($q^2 > 0.5$, $r^2 > 0.9$, $r^2_{pred} > 0.5$) [36, 37].

Visual illustrations of the 3D-QSAR were performed through contour maps, generated in a 3D grid orientation of 80% favourable and 20% unfavourable field contributions. Contour maps give the idea about favourable and unfavourable regions around the molecules. Structural modification, according to the contour map analysis, helps in the alteration of physicochemical properties that might be responsible for increasing or decreasing the potency of molecules [38].

In MDS studies, a chain of co-crystallised ligand of telomerase (PDB: 5CQG) was stabilised in the presence of Amber14sb force field for 50 ns with a time step of 2 fs [39]. During the simulation process, protein structure was stabilised at 1-atm pressure with an average temperature of 299.98 k and potential energy of 1,145,336 kJ/m converged in 997 steps using GROMACS 2019.4 software. For the determination of molecular interactions of the highest active compound with simulated/unsimulated protein structure [40], molecular docking was carried out in SurFlex dock module of SYBYL-X. Based upon all studies, few novel quinoline

and acridine derivatives were designed and docked on the same target to evaluate their comparative potentials.

Overall, in this study, we performed the 3D-QSAR and molecular dynamics/simulation-assisted molecular docking studies of known reported telomerase inhibitors to identify potential spatial features for designing novel telomerase inhibitors and also designing few novel molecules.

Results and discussion

The experimental and predicted activity values of the CoMFA/CoMSIA are listed in Table 3, and a correlation between experimental and predicted pIC_{50} is shown in Fig. 3. Here, the correlation analysis of experimental and predicted pIC_{50} value was explained by the linearity graph. In this graph, the experimental pIC_{50} was used as the logarithmic values of the biological activity (IC_{50}) of selected molecules as reported in the literature and the predicted pIC_{50} generated through the CoMFA and CoMSIA PLS analysis. During the linearity analysis, it was observed that the CoMSIA analysis showed better linearity between both the parameters with the observed R^2 value of 0.7403, but in case of the CoMFA, the linear relationship between the experiment and predicted

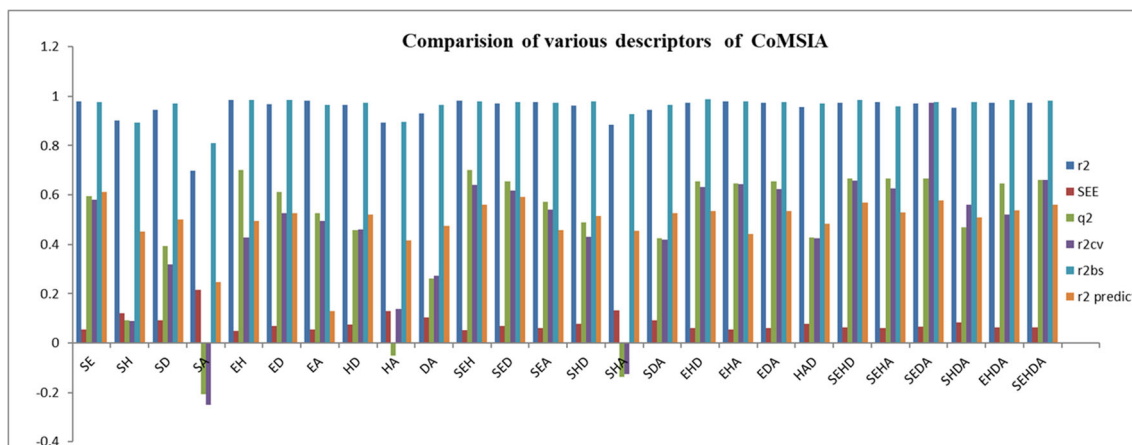


Fig. 4 Comparison of CoMSIA descriptors' results

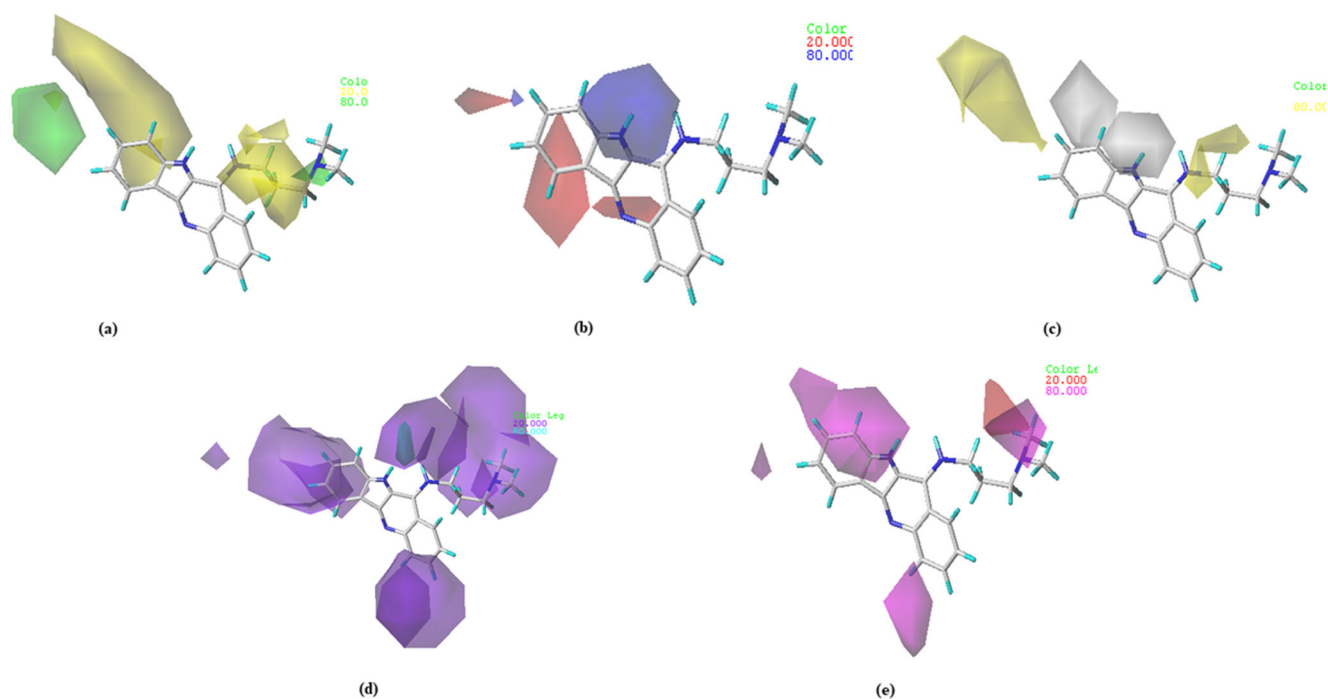


Fig. 5 CoMSIA contour maps with structure of compound 3 shown inside the field. **a** CoMSIA steric contour map: favourable region refers to green colour while yellow colour refers to a disfavourable region; **b** CoMSIA electrostatic contour map: red colour represents negatively charged and blue represents positively charged substituents; **c**

hydrophobic field: yellow colour refers to favourable and white colour refers to disfavourable substitution; **d** hydrogen bond donor field: cyan and purple colours refer to favourable and disfavourable, respectively; **e** hydrogen bond acceptor field: magenta and red colour contour map supports favourable and disfavourable substitutions

pIC_{50} was observed lower with the R^2 value of 0.6546. The graph helped to validate the predictive power of the generated QSAR model. In this study, statistical outcomes of the CoMFA was found to be lower than the standard limits; therefore, the statistical significance of the CoMSIA was utilised for the generation of the QSAR model [12, 17].

The CoMSIA models with good statistical values were generated by permutation combination of all descriptors, viz. steric, electrostatic, hydrophobic and donor as well as acceptor fields. The statistical results of all descriptors' combination of

the CoMSIA model are shown in Fig. 4 (and also in Supplementary Information Table ST-1). From all these descriptors' combinations, SEHD (steric, electrostatic, hydrophobic and donor) showed best statistical results with q^2 value of 0.667, r^2 value of 0.975, r^2_{cv} value of 0.659, r^2_{bs} value of 0.988, F value of 134.336, SEE value of 0.062 and r^2_{pred} value of 0.570. Combination of SEHDA (steric, electrostatic, hydrophobic, donor and acceptor) also showed almost equivalent result as SEHD with q^2 value of 0.662, r^2 value of 0.974, r^2_{cv} value of 0.660, r^2_{bs} value of 0.981, F value of 129.633, SEE

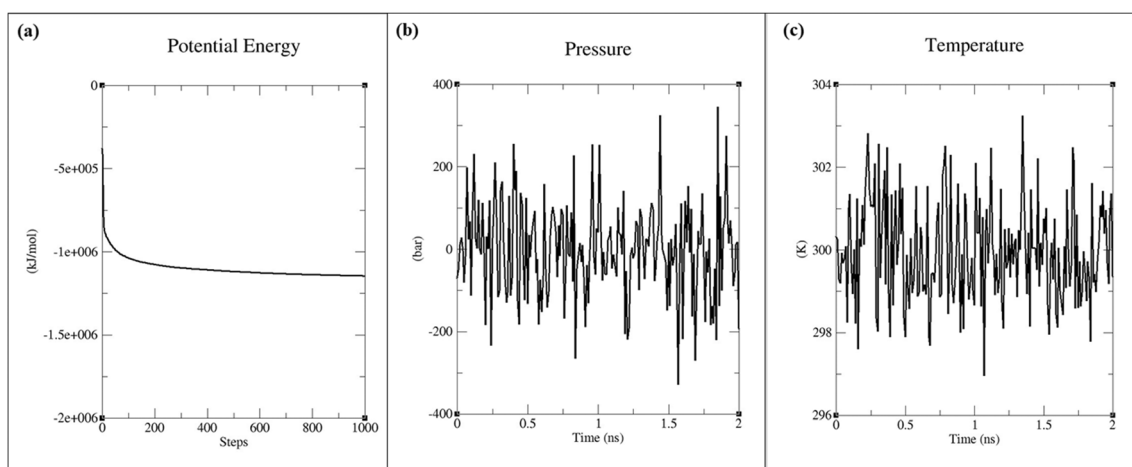


Fig. 6 MDS study of a chain of telomerase (PDB ID: 5CQG) concerning **a** potential energy versus time; **b** pressure versus time; **c** temperature versus time

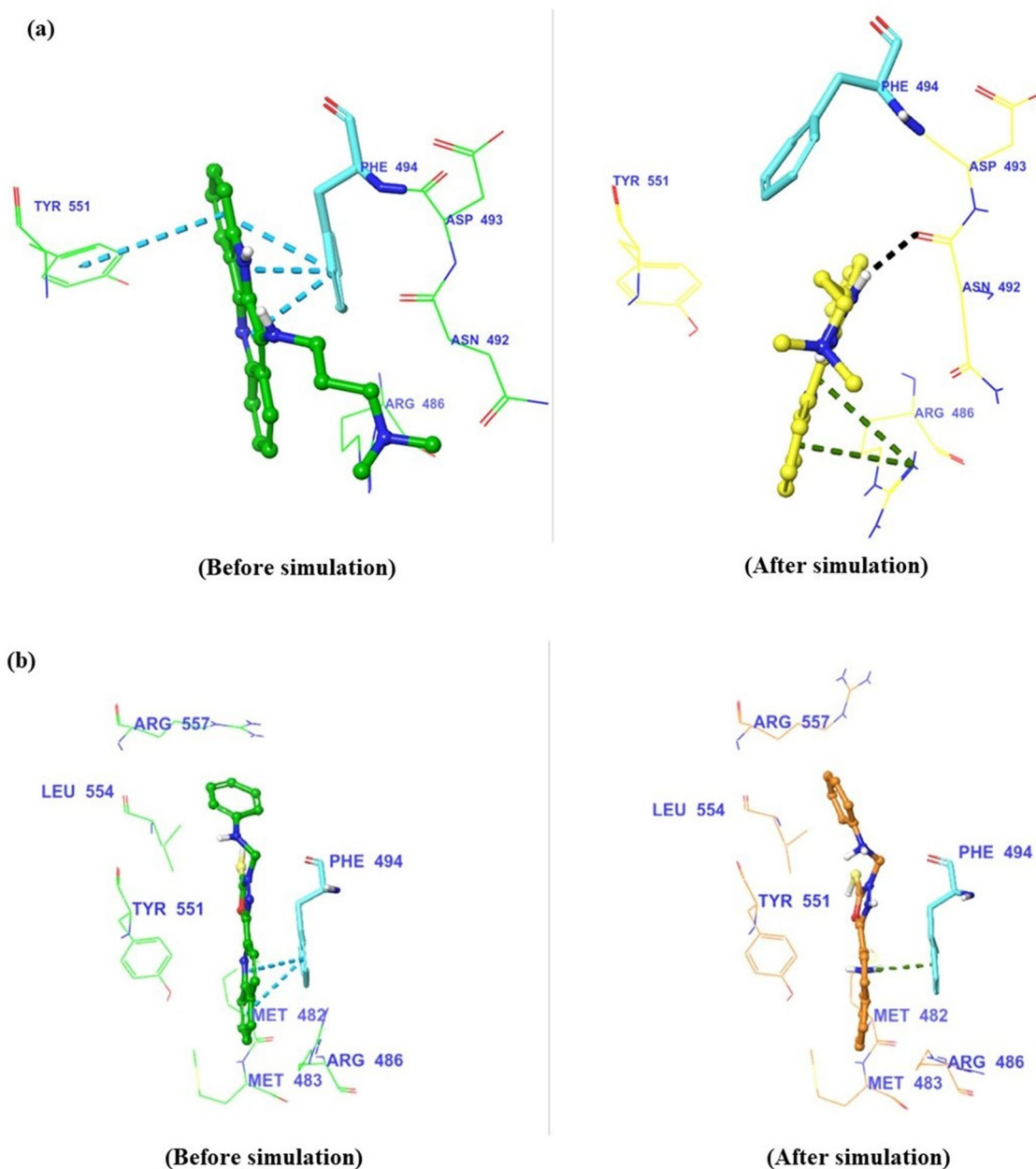


Fig. 7 Effect of MDS analysis over the active and inactive ligand. **a** MDS study of compound 3; **b** MDS study of compound 11

value of 0.063 and r^2_{pred} value of 0.560, with the field contribution value of 0.093, 0.217, 0.193, 0.384 and 0.113 for steric, electrostatic, hydrophobic, donor and acceptor field, respectively. Because SEHDA combination covered all the fields as well as it gave optimum statistical results, this combination was utilised for the generation and analysis of counter maps.

Highly potent molecule (molecule 3) overlaid on the contour maps of steric, electrostatic, hydrophobic, donor and acceptor fields as shown in Fig. 5. Based on favourable and disfavourable regions, the contour map analysis was performed. As shown in Fig. 5a of a steric contour map, the green colour referred to the favoured region and the yellow colour indicated disfavourable region for bulky group substitution

which could be explained by a comparison of compounds 3 and 9. Compound 3 (IC_{50} value of 0.44 μM) consisted of the methyl-substituted aliphatic amide side chain at the 4th position of the quinoline ring which was found to be sterically favourable due to the presence of $-\text{CH}_3$ group. Compared to compound 3, compound 9 with less bulky and polar $-\text{OH}$ substitution was found to be significantly less potent (IC_{50} value of 12.3 μM). This was also proved by the comparison of compounds 14 and 11; where substitution of *o*-fluoro benzamide-oxadiazole at 2nd position of quinoline ring in compound 14 was responsible for higher potency (IC_{50} value of 0.8 μM) as compared to compound 11 where benzamide-oxadiazole-linked quinoline moiety showed lower potency

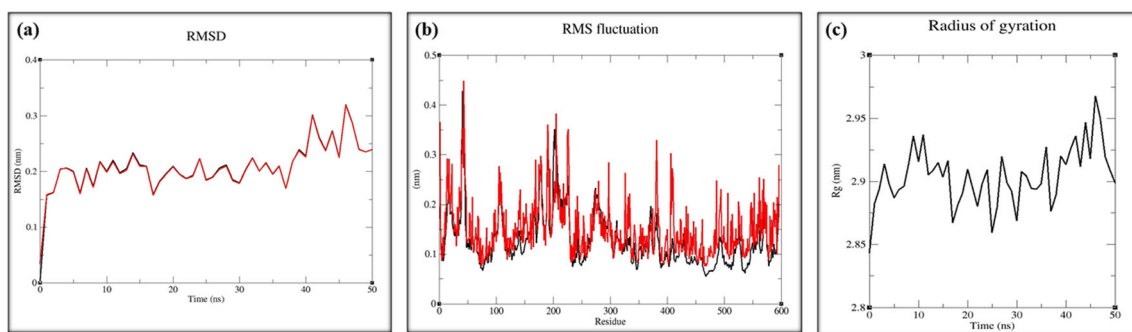


Fig. 8 Analysis of molecular simulation study. **a** Backbone RMSD of 5CQG: unstimulated protein is represented by the black colour while simulated protein is represented by the red colour; **b** RMSF per residue

of 5CQG with its variants: black colour represents the fluctuation in presence of active variant and red colour represents the fluctuation in presence of inactive variants; **c** Measure of Rg after simulation

(IC_{50} value of 12.8 μM). CoMSIA electrostatic contour map is shown in Fig. 5b. Here, the blue colour region favoured electropositive substitutions while red colour favoured electronegative substitutions. Substitution of electropositive $-\text{NH}$ of indole ring at 3rd position of quinoline ring favoured the activity while electronegative oxygen of benzofuran at the same position decreased the activity. This was confirmed by all selected molecules of series one. Thus, it is concluded throughout the series that negatively charged nitrogen atom, which is present in the quinoline ring, is essential for its activity and the same is confirmed by the red colour contour map. Additionally, electronegative halide substitution is also favourable for the activity which is supported by compound 14 (IC_{50} value of 0.8 μM).

In the hydrophobic contour map, the yellow colour region favoured hydrophobic substitution while white colour favoured hydrophilic substitution, which is shown in Fig. 5c. The contour map of the hydrophobic region was validated by compounds 1 and 10. In compound 1, the substitution of nonpolar morpholinoethanamide side chain favoured activity (IC_{50} value of 0.5 μM) while polar aminoethanol substitution in compound 10 disfavoured activity (IC_{50} value of 8.1 μM). The abovementioned

compounds additionally helped in cross-validation of the electrostatic contour map, where hydrophilic contour map was shown in place of electropositive region or in the place of $-\text{NH}$ substitution. Donor field contributors are shown in Fig. 5d, where the cyan colour represented favourable donor substitution while purple colour represented the substitution of disfavour electron donor group. Amine group of indole at 3rd position of quinoline moiety favoured electron donor property as found in compounds 1 to 5. Electropositive and hydrophilic contour maps sympathetically supported to favourable donor substitution. All selected molecules are comprised of electronegative nitrogen atom which was responsible for disfavoured donor field contribution. Contour map of the CoMSIA acceptor field is shown in Fig. 5e, where the magenta and the red colour region represented favourable and disfavoured substitutions, respectively. Acceptor region was validated by compounds 12 and 19. In the case of compound 19, *p*-chloromethyl aniline favoured the activity due to the presence of electron-withdrawing halide group (IC_{50} value of 0.9 μM). In contrast, electron-donating methyl atom of dimethylaniline in compound 12 disfavoured the activity (IC_{50} value of 7.3 μM).

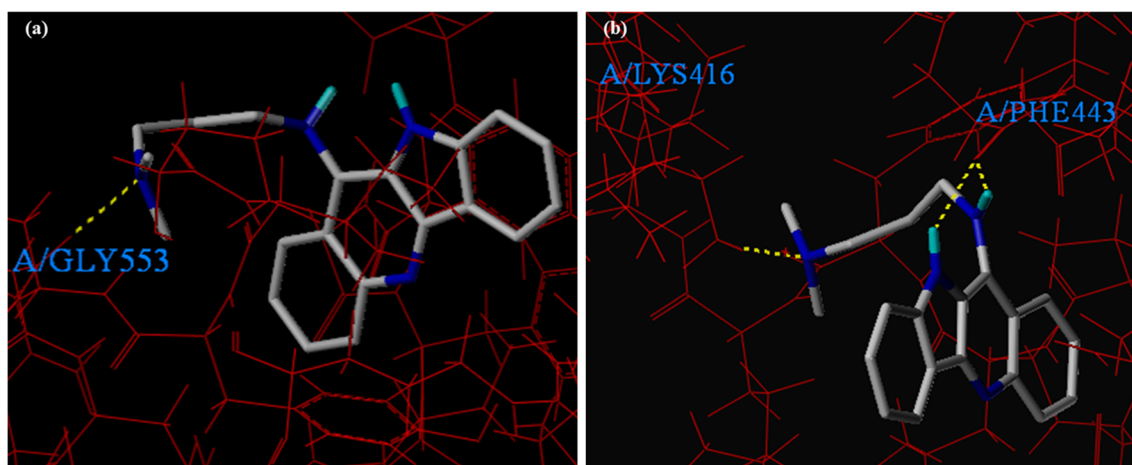
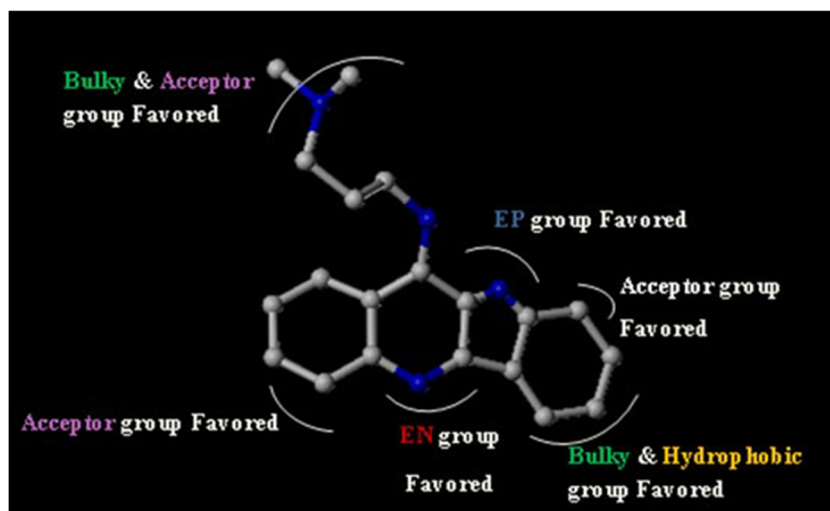


Fig. 9 Docking interactions of highest active ligand with **a** simulated and **b** unstimulated protein structure (PDB-5CQG)

Fig. 10 Important structural requirements of quinoline moieties as per the ligand-based 3D-QSAR and structure-based MDS-assisted molecular docking study



Additionally, in the case of compounds 1, 6 and 24; electron-withdrawing oxygen atom of the morpholine ring supported the acceptor region and activity.

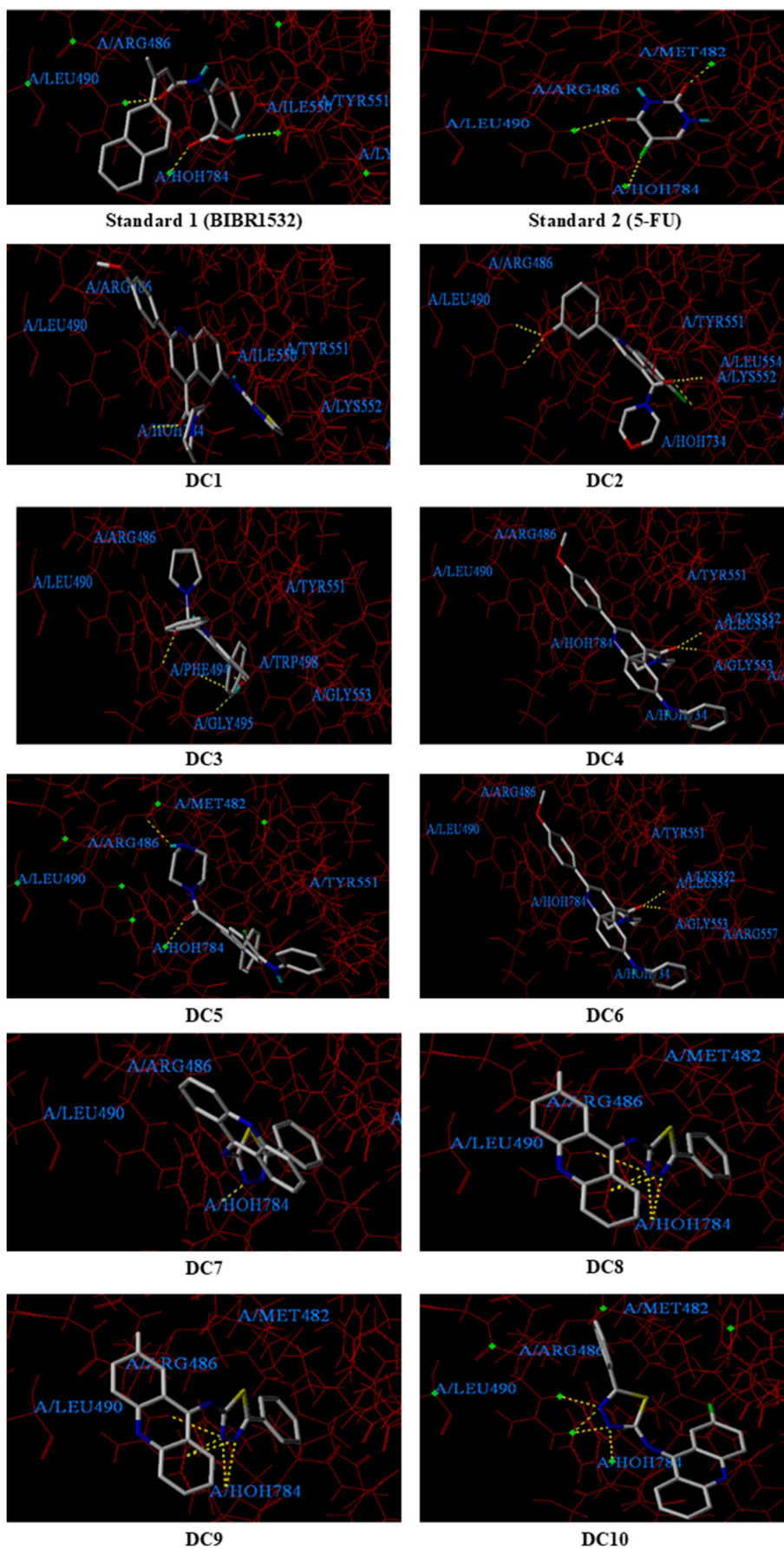
During MDS study, effects of concerned pressure, temperature and potential energy over the stabilisation of protein at a particular time duration were observed, as shown in Fig. 6. The binding site residues, at around 6 Å of the ligand, were compared for compounds 3 and 11, before and after MD simulation and are shown in Fig. 7. In the case of compound 3, the ligand showed better interaction affinity towards the protein which was significantly changed with the change in dynamic environment of protein. The tail of the ligand displaced towards the exposed solvent and the main core of the ligand mainly lied towards the hydrophobic pocket. Before the simulation, the compound showed the pi-stacking interactions with the residue of Phe494 and Tyr551 which was absent at the 50-ns pose and it might be due to the fluctuations in amino acid sequences. The compound showed pi-cation interaction with Arg486, and the –NH of fused indole ring showed the H-bond interaction with the carbonyl group of Asn492 at the distance of 2.05 Å after the simulation. The compound 11 showed low interaction affinity towards the target as it showed only a single pi-interaction with Phe494 and none of the significant changes in the interaction was observed after the simulation. The findings suggested that the changes in the dynamic environment of the protein led the variation in ligand-protein interaction affinity, which helped to gain an idea about the phenomenon behind ligand designing for the significant inhibition.

Furthermore, the reliability of the molecular dynamic studies was checked through the RMSD, RMSF and Rg analysis, as shown in Fig. 8. Resultant RMSD analysis is shown in Fig. 8a. Here, similar alignments of simulated and unsimulated protein with zero RMSD value helped to understand that the amino acid sequence of the unsimulated protein remained unchanged after simulation.

Effect of active compound 3 and comparatively inactive compound 11 variants of selected QSAR series over the flexibility of simulated protein were analysed by the RMSF analysis as shown in Fig. 8b. Less fluctuations in the presence of compound 3 indicated more stable conformer, whereas more fluctuations in the presence of compound 11 indicated less stable conformer. The measure of the compactness of protein by the Rg analysis is shown in Fig. 8c where the Rg values were reasonably unchanged in their compact (folded) region over the course of 50 ns at 300 k, which defined that the structure of the protein was stable in the dynamic environment. Amino acid sequencing was rechecked with the help of the Ramachandran Plot (Supplementary Information as Figure SF-1). The resultant similarity of simulated and unsimulated protein was the number of residues in the favourable region 1103 (92.8%), the number of residues in the allowed region 68 (5.7%) and the number of residues in the outlier region 17 (1.4%). This explained that the amino acid sequence of unsimulated protein remained unchanged after the simulation.

Molecular docking studies of the active ligand with unsimulated and simulated proteins are shown in Fig. 9, and they supported cross-validation of the CoMSIA contour maps. Docking of compound 3 with unsimulated and simulated proteins showed the interactions of nitrogen atom of alkyl amide side chain with hydrophobic Gly553 and positive charge Lys416, respectively. These interactions explained the importance of the hydrogen bond acceptor and favourable hydrophobic interactions in this region which was supported by magenta colour contour map of acceptor field around nitrogen atom. After simulation, the number of hydrogen bond interactions increased as the –NH– of indole ring substituted at 3rd position and –NH– substituted at 4th position of quinoline core moiety interacted with Phe443. These interactions supported an electropositive functional group required for the activity

Fig. 11 Docking interactions of potent molecules along with design compounds



which was validated by the blue colour counter map around these 'N' atom. Based on the 3D-QSAR studies and MDS-assisted molecular docking studies, the essential structural requirements of quinoline moiety is shown in Fig. 10.

By utilising overall data of the study, we have designed ten molecules, five with quinoline and five with acridine as core moiety. All designed molecules were docked in A-chain of telomerase active site (PDB-5CQG) in SurFlex Dock module in SYBYL (results are shown as Supplementary Information Table ST-2). Docking interactions of potent molecules along with design compounds are shown in Fig. 11. Comparative docking study of the designed molecules with marketed anticancer drug 5-FU and standard anti-telomerase agent BIBR1532 was also performed. The designed molecules showed better interaction affinity than marketed drug and it is similar to BIBR1532. As the same in BIBR1532, in the design molecules, negatively charged oxygen was facing positively charged Arg484.

Conclusion

This study is an attempt to design novel compounds with potent telomerase inhibitory activity. Statistically significant CoMSIA with a q^2 value of 0.662 and higher predictability with an r^2_{pred} value of 0.560 was utilised in the generation of contour maps. Substitution of steric, electrostatic, hydrophobic and acceptor and donor atoms is significant to inhibit the effect of telomerase enzyme. Molecular dynamic and simulation-aided molecular docking study assisted the identification of promising features of quinoline moiety for telomerase inhibition. It was also observed that the improvement of hydrogen bond interactions resultant from a conformational change in protein structure was not due to the changes in amino acid sequences. The generated 3D-QSAR model helped to introduce a new direction in designing novel quinoline and acridine derivatives while molecular docking helped to investigate the possible binding interactions of design molecules which could be explored in future.

Supplementary Information The online version contains supplementary material available at <https://doi.org/10.1007/s00894-020-04648-2>.

Acknowledgements Authors are thankful to Nirma University, Ahmedabad, India, for supporting work, which is a part of Doctor of Philosophy (PhD) research work of Keerti Vishwakarma, to be submitted to Nirma University, Ahmedabad, India.

Authors' contributions Keerti Vishwakarma: conceptualization; methodology and validation; data curation; writing—original draft

Hardik Bhatt: conceptualization; reviewing the methodology, results, and discussion; editing—final draft

References

- Puri N, Girard J (2013) Novel therapeutics targeting telomerase and telomeres. *J Cancer Sci Ther* 5:1–3. <https://doi.org/10.4172/1948-5956.1000e127>
- Tang H, Wang H et al (2018) HuR regulates telomerase activity through TERC methylation. *Nat Commun* 9:1–12. <https://doi.org/10.1038/s41467-018-05213-5>
- Ganesan K, Xu B (2018) Telomerase inhibitors from natural products and their anticancer potential. *Int J Mol Sci* 19. <https://doi.org/10.3390/ijms19010013>
- Jäger K, Walter M (2016) Therapeutic targeting of telomerase. *Genes (Basel)*. 7 1–24. <https://doi.org/10.3390/genes7070039>
- Agrawal A, Dang S, Gabrani R (2012) Recent patents on anti-telomerase cancer therapy. *Recent Pat. Anti-cancer. Drug Discov* 7:102–117. <https://doi.org/10.2174/157489212798357958>
- Zhang L, Huang J, Ren L et al (2008) Synthesis and evaluation of cationic phthalocyanine derivatives as potential inhibitors of telomerase. *Bioorg Med Chem* 16:303–312. <https://doi.org/10.1016/j.bmc.2007.09.037>
- Wang J, Liu L, Ma H (2017) Sensors and actuators B: chemical label-free real-time investigation of the effect of telomerase inhibitors based on quartz crystal microbalance measurement. *Sensors Actuators B Chem* 239:943–950. <https://doi.org/10.1016/j.snb.2016.08.021>
- Seimiya H, Oh-Hara T, Suzuki T et al (2002) Telomere shortening and growth inhibition of human cancer cells by novel synthetic telomerase inhibitors MST-312, MST-295, and MST-199 1. *Mol Cancer Ther* 1:657–665 <http://mct.aacrjournals.org/content/molcanther/1/9/657.full.pdf>. Accessed 29 Dec 2017
- Drewe WC, Nanjunda R, Gunaratnam M et al (2008) Rational design of substituted diarylureas: a scaffold for binding to G-quadruplex motifs. *J Med Chem* 51:7751–7767. <https://doi.org/10.1021/jm801245v>
- Wang Y, Cheng FX, Yuan XL et al (2016) Dihydropyrazole derivatives as telomerase inhibitors: structure-based design, synthesis, SAR and anticancer evaluation in vitro and in vivo. *Eur J Med Chem* 112:231–251. <https://doi.org/10.1016/J.EJMECH.2016.02.009>
- Verma J, Khedkar VM, Coutinho EC (2010) 3D-QSAR in drug design—a review. *Curr Top Med Chem* 10:95–115. <https://doi.org/10.2174/156802610790232260>
- Zambre VP, Murumkar PR, Giridhar R, Yadav MR (2010) Development of highly predictive 3D-QSAR CoMSIA models for anthraquinone and acridone derivatives as telomerase inhibitors targeting G-quadruplex DNA telomere. *J Mol Graph Model* 29: 229–239. <https://doi.org/10.1016/j.jmgm.2010.07.003>
- Halim SA, Ul-Haq Z (2015) Structure based 3D-QSAR studies of Interleukin-2 inhibitors: comparing the quality and predictivity of 3D-QSAR models obtained from different alignment methods and charge calculations. *Chem Biol Interact* 238:9–24. <https://doi.org/10.1016/j.cbi.2015.05.018>
- Feng K, Ren Y, Li R (2017) Combined pharmacophore-guided 3D-QSAR, molecular docking and molecular dynamics studies for evodiamine analogs as DNA topoisomerase I inhibitors. *J. Taiwan Inst. Chem Eng* 78:81–95. <https://doi.org/10.1016/j.jtice.2017.06.027>
- Patel B. D, Ghate M. D, (2015) 3D-QSAR studies of dipeptidyl peptidase-4 inhibitors using various alignment methods. *Med Chem Res* 24:1060–1069. <https://doi.org/10.1007/s00044-014-1178-7>.
- Ismail S, Mohamed AO, Abdel F et al (2012) CoMFA and CoMSIA Studies of 1,2-dihydropyridine derivatives as anticancer agents. *Med Chem (Los Angeles)* 8(2012):372–383. <https://doi.org/10.1097/COC.0b013e3182a79009.Pain>

17. Balupuri A, Balasubramanian PK, Cho SJ (2017) 3D-QSAR, docking, molecular dynamics simulation and free energy calculation studies of some pyrimidine derivatives as novel JAK3 inhibitors. *Arab J Chem* 9:1–20. <https://doi.org/10.1016/j.arabjc.2017.09.009>
18. Alamri MA (2020) Pharmacoinformatics and molecular dynamic simulation studies to identify potential small-molecule inhibitors of WNK-SPAK/OSR1 signaling that mimic the RFQV motifs of WNK kinases. *Arab J Chem* 13:5107–5117. <https://doi.org/10.1016/j.arabjc.2020.02.010>
19. Sargsyan K, Grauffel C, Lim C (2017) How molecular size impacts RMSD applications in molecular dynamics simulations. *J Chem Theory Comput* 13:1518–1524. <https://doi.org/10.1021/acs.jctc.7b00028>
20. Ho BK, Brasseur R (2005) The Ramachandran plots of glycine and pre-proline. *BMC Struct Biol* 5:1–11. <https://doi.org/10.1186/1472-6807-5-14>
21. Fan Z, Ho S, Wen R et al (2019) Design, synthesis and molecular docking analysis of flavonoid derivatives as potential. *Molecules* 24:1–14. <https://doi.org/10.3390/molecules24173180>
22. Pereira GRC, Tavares GDB, Freitas MC, Mesquita JF (2020) In silico analysis of the tryptophan hydroxylase 2 (TPH2) protein variants related to psychiatric disorders. *PLoS One* 15:1–23. <https://doi.org/10.1371/journal.pone.0229730>
23. Pagadala NS, Syed K, Tuszynski J (2017) Software for molecular docking: a review. *Biophys Rev* 9:91–102. <https://doi.org/10.1007/s12551-016-0247-1>
24. Duan Y, Yao Y, Tang D (2014) Synthesis and biological evaluation of quinoline–imidazole hybrids as potent telomerase inhibitors: a promising class of antitumor agents, *R Soc Chem* 420382–20392. <https://doi.org/10.1039/c4ra01936a>
25. Zhou J, Lu Y, Ou T, Zhou J, Huang Z, Zhu X, Du C (2005) Synthesis and evaluation of quindoline derivatives as g-quadruplex inducing and stabilizing ligands and potential inhibitors of telomerase. *J Med Chem* 48:7315–7321. <https://doi.org/10.1021/jm050041b>
26. Sun J, Zhu H, Yang Z, Zhu H (2013) Synthesis, molecular modeling and biological evaluation of 2-aminomethyl-5-anticancer agent, *Eur J Med Chem* 6023–28. <https://doi.org/10.1016/j.ejmech.2012.11.039>
27. Harrison RJ, Gowan SM, Kelland LR, Neidle S (1999) Human telomerase inhibition by substituted acridine derivatives, *Bioorganic Med. Chem Lett* 9:2463–2468. [https://doi.org/10.1016/S0960-894X\(99\)00394-7](https://doi.org/10.1016/S0960-894X(99)00394-7)
28. Borisa A, Bhatt H (2015) 3D-QSAR (CoMFA, CoMFA-RG, CoMSIA) and molecular docking study of thienopyrimidine and thienopyridine derivatives to explore structural requirements for aurora-B kinase inhibition. *Eur J Pharm Sci* 79:1–12. <https://doi.org/10.1016/j.ejps.2015.08.017>
29. Yadav DK, Saloni, Sharma P et al (2017) Studies of the benzopyran class of selective COX-2 inhibitors using 3D-QSAR and molecular docking. *Arch Pharm Res* 1–12. <https://doi.org/10.1007/s12272-017-0945-7>
30. Chekkara R, Kandakatla N, Gorla VR et al (2017) Theoretical studies on benzimidazole and imidazo[1,2-a] pyridine derivatives as Polo-like kinase 1 (Plk1) inhibitors: pharmacophore modeling, atom-based 3D-QSAR and molecular docking approach. *J Saudi Chem Soc* 21:S311–S321. <https://doi.org/10.1016/j.jscs.2014.03.007>
31. Bryan C, Rice C, Harkisheimer M et al (2015) Structural basis of telomerase inhibition by the highly specific BIBR1532. *Struct Des* 23:1934–1942. <https://doi.org/10.1016/j.str.2015.08.006>
32. Diaz A, Martínez E, Puerta L et al (2014) A CoMSIA study to design antagonist ligands for the LuxS protein, *New J. Chem.* 38: 1235–1249. <https://doi.org/10.1039/c3nj01162c>
33. Chaube U, Chhatbar D, Bhatt H (2016) 3D-QSAR, molecular dynamics simulations and molecular docking studies of benzoxazepine moiety as mTOR inhibitor for the treatment of lung cancer. *Bioorg Med Chem Lett* 26:864–874. <https://doi.org/10.1016/j.bmcl.2015.12.075>
34. Gao J, Sun J, Wang T, Sheng S, Huang T (2017) Combined 3D-QSAR modeling and molecular docking study on spiro-derivatives as inhibitors of acetyl-CoA carboxylase. *Med Chem Res* 26:361–371. <https://doi.org/10.1007/s00044-016-1743-3>
35. Duan YT, Yao YF, Tang DJ (2014) Synthesis and biological evaluation of quinoline-imidazole hybrids as potent telomerase inhibitors: a promising class of antitumor agents. *Rsc Adv* 4:20382–20392. <https://doi.org/10.1039/c4ra01936a>
36. Wang JL, Cheng LP, Wang TC, Deng W, Wu FH (2017) Molecular modeling study of CP-690550 derivatives as JAK3 kinase inhibitors through combined 3D-QSAR, molecular docking, and dynamics simulation techniques. *J Mol Graph Model* 72:178–186. <https://doi.org/10.1016/j.jmgm.2016.12.020>
37. Zhu J, Ke K, Xu L, Jin J (2019) Theoretical studies on the selectivity mechanisms of PI3K δ inhibition with marketed idelalisib and its derivatives by 3D-QSAR, molecular docking, and molecular dynamics simulation. *J Mol Model* 25. <https://doi.org/10.1007/s00894-019-4129-x>
38. Murumkar P, Sharma MK, Miniyar P. B, Yadav M. R (2016) Development of a credible 3D-QSAR CoMSIA model and docking studies for a series of triazoles and tetrazoles containing 11 β -HSD1 inhibitors, *SAR QSAR Environ Res* 1–28. <https://doi.org/10.1080/1062936X.2016.1167774>
39. Shirgahi TF, Bagherzadeh K, Golestanian S, Jarstfer M (2015) Potent Human telomerase inhibitors: molecular dynamic simulations, multiple pharmacophore-based virtual screening, and biochemical assays. *J Chem Inf Model* 55:2596–2610. <https://doi.org/10.1021/acs.jcim.5b00336>
40. Fuggetta MP, De Mico A, Cottarelli A et al (2016) Synthesis and enantiomeric separation of a novel spiroketal derivative: a potent human telomerase inhibitor with high in vitro anticancer activity. *J Med Chem* 1–49. <https://doi.org/10.1021/acs.jmedchem.6b01046>

Publisher's note Springer Nature remains neutral with regard to jurisdictional claims in published maps and institutional affiliations.